Appendix 2

Concordia diagrams

Figure A1 shows Tera-Wasserburg concordia diagrams for detrital zircon in the young sediments, data from Appendix 1 in supplementary material.

(**a**) Zircons from sediments of the Maputaland Group.

(**b**) Zircons from Recent stream sediments on Karoo dolerite, Mesoproterozoic granite and gneiss and beach sand.

(**c**) Zircons from Recent sediments deposited on Archaean basement rocks. Note that Archaean zircons in sample SA12/32 are shown in an inset at higher $^{207}Pb/^{206}Pb$ ratio than the main part of the diagram.

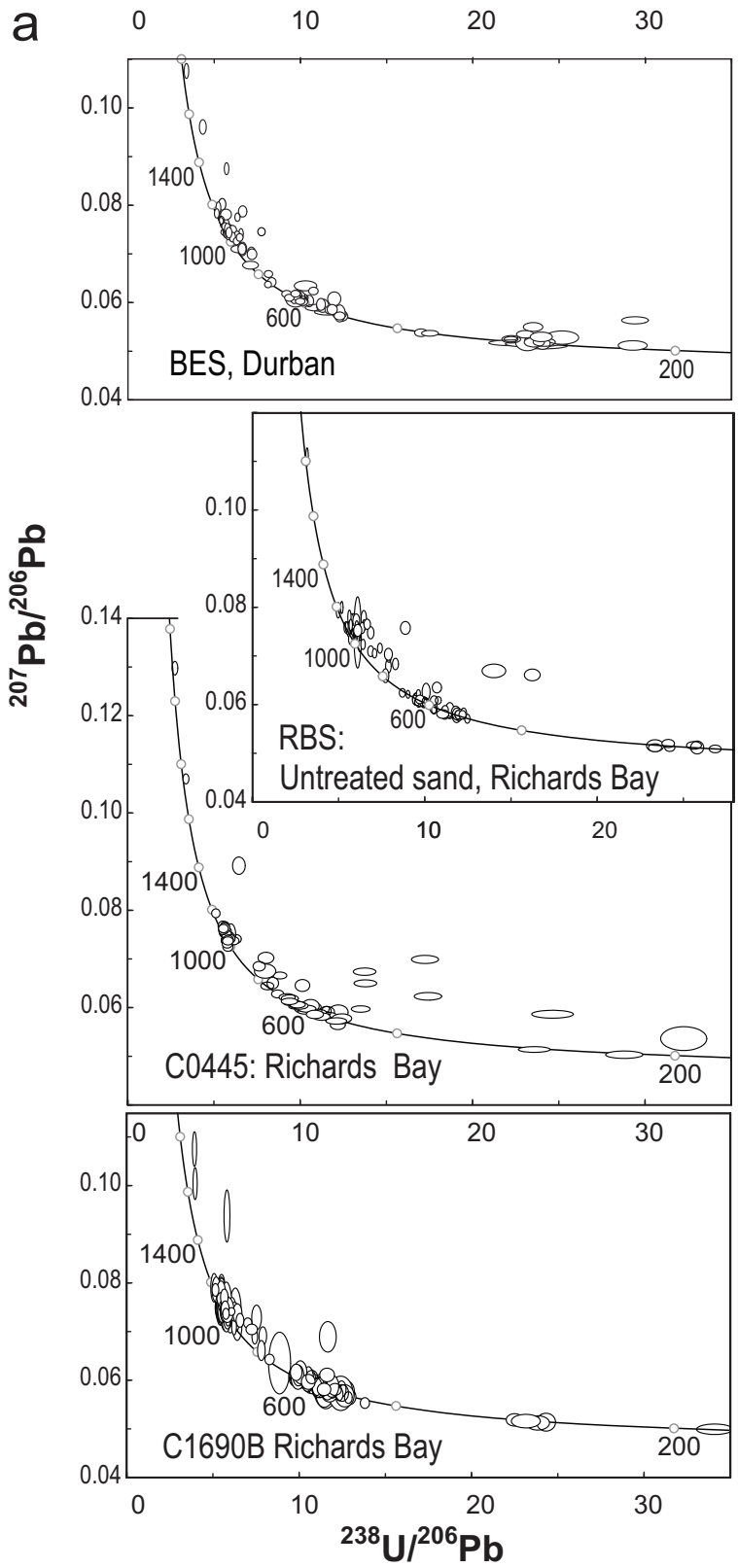
a
0
10
20
30
0.10
0.08
0.06
0.04
1400
1000
600
200
BES, Durban
RBS:
Untreated sand, Richards Bay
0.14
0.12
C0445: Richards Bay
C1690B Richards Bay
$^{207}Pb/^{206}Pb$
$^{238}U/^{206}Pb$

Figure A1a

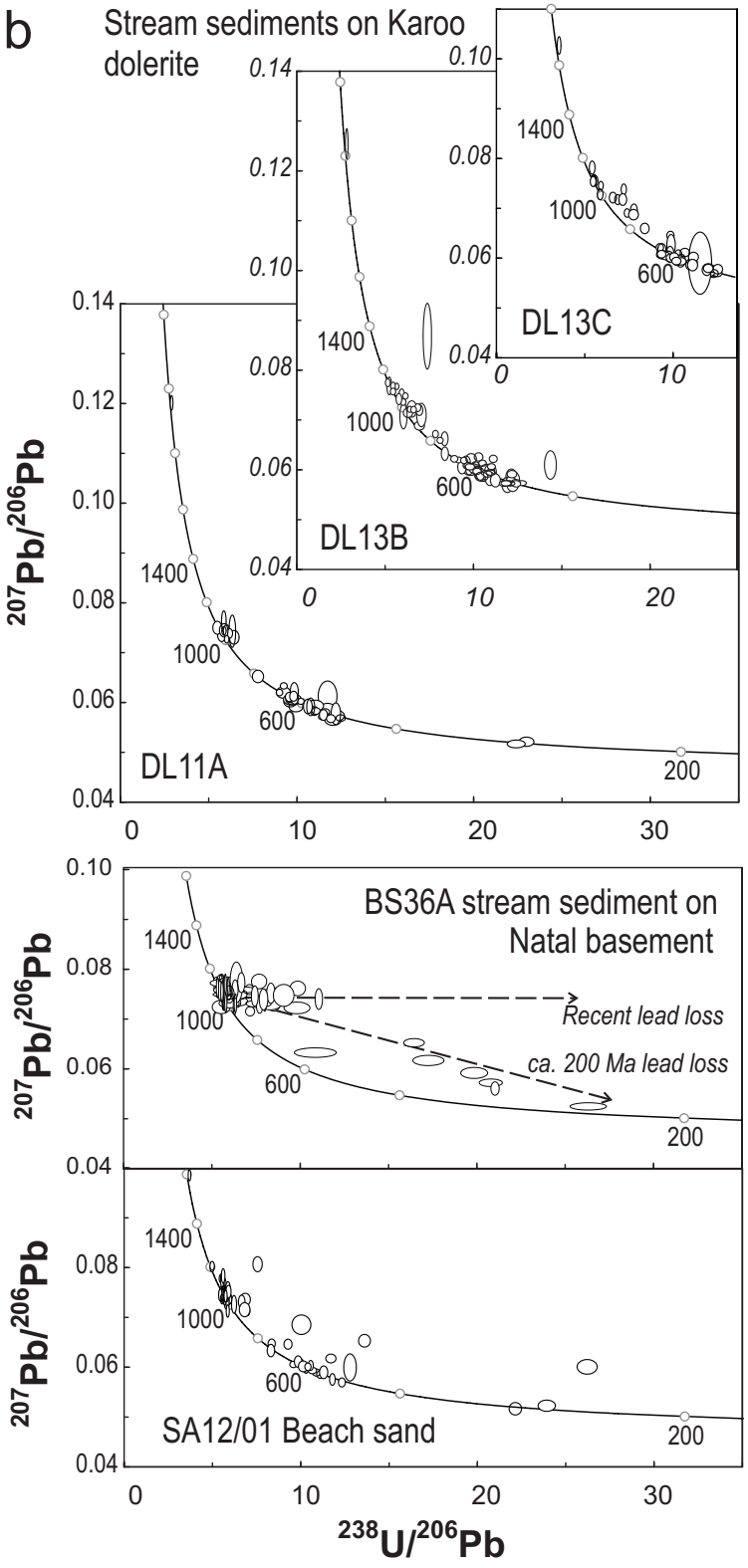
b
Stream sediments on Karoo dolerite
DL11A
DL13B
DL13C
BS36A stream sediment on Natal basement
Recent lead loss
ca. 200 Ma lead loss
SA12/01 Beach sand
1400
1000
600
200
$^{207}Pb/^{206}Pb$
$^{238}U/^{206}Pb$

Figure A1b

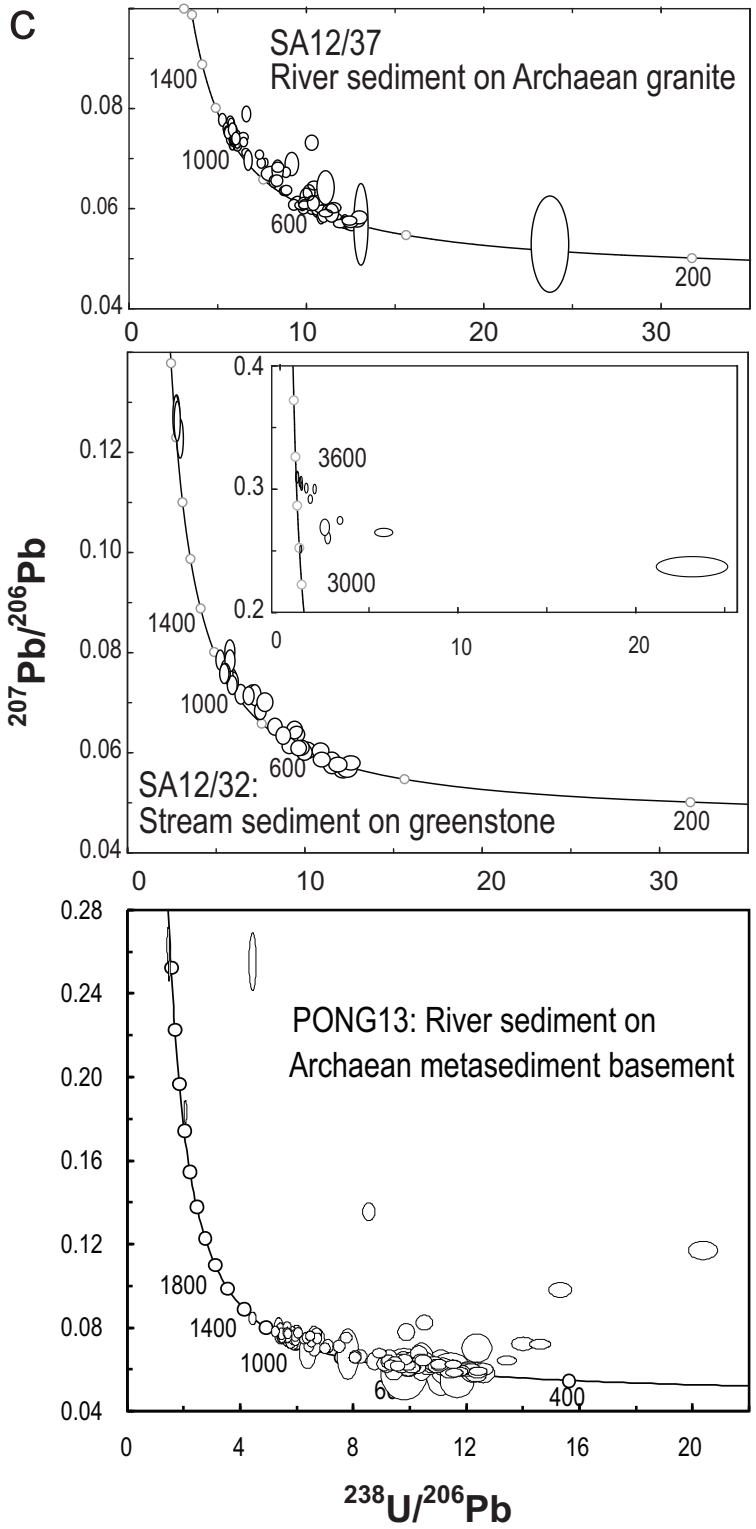
C
SA12/37
River sediment on Archaean granite
1400
1000
600
200
0.08
0.06
0.04
0
10
20
30
0.4
0.3
0.2
3600
3000
0.12
0.10
SA12/32:
Stream sediment on greenstone
0.28
0.24
0.20
0.16
PONG13: River sediment on
Archaean metasediment basement
1800
400
207Pb/206Pb
238U/206Pb

Figure A1c

Effects of discordance

Zircons may be discordant because of loss of radiogenic lead after crystallization or because of the presence of uncorrected common lead (Andersen 2002, Gehrels 2012). In the present case, common lead has, as far as possible, been removed by a conventional common lead correction based on the observed $^{204}Pb/^{206}Pb$ ratio, so the residual discordance in grains reported in Appendix 1 is due to lead loss. Lead-loss discordance causes observed $^{206}Pb/^{238}U$ and $^{207}Pb/^{235}U$ ratios (and hence the corresponding ages) to be lower than the undisturbed values. If lead loss has taken place in the geological past (ancient lead loss), the $^{207}Pb/^{206}Pb$ ratio (and age) is also affected. In eastern South Africa, a significant thermal event at ca. 180 Ma related to Karoo magmatism and breakup of Gondwana may have caused lead loss effects also for the $^{207}Pb/^{206}Pb$ age.

Two of our samples which have yielded a significant fraction of zircon showing lead-loss effects will be used as examples here: *SA12/32* and *BS36A*.

For the Archaean age fraction in *SA12/32*, ancient lead-loss, probably of Mesozoic age caused in part severe discordance. Projecting these grains back to the concordia from the origin (i.e. calculating the $^{207}Pb/^{206}Pb$ age) results in ages in the range 3000-3200 Ma (Fig. A2a), suggesting the existence of a late Palaeoarchaean to early Mesoarchaean age fraction in this sample. The concordant (i.e. less than 10 % normally discordant) grains do not show indications of such a fraction. This apparent age fraction is a result of significant loss of radiogenic lead in an event that is sufficiently old to affect the $^{207}Pb/^{206}Pb$ age. Effects of this lead loss event is seen also in ca. 3.55 Ga basement rocks from the same area (Jele, 2014), and in many rocks from other parts of the Kaapvaal Craton (e.g. Zeh et al., 2010, 2011, 2013)

In contrast, *BS36A* has a single Mesoproterozoic age fraction (1000-1150 Ma), overprinted by both Mesozoic and Recent lead loss (Fig. A2b).The origin of zircon in this sample may be from ca. 1.15 -1.20 Ga gneisses and granitic intrusions of the Mzumbe terrane of the Natal sector (McCourt *et al.* 2006; Spencer *et al.* 2015). Lead-loss has spread the affected zircons out in a field limited by lead-loss lines to lower intercepts at 0 and ca. 200 Ma. The effect is most severe in the $^{206}Pb/^{238}U$ age (Fig.

A2b) – if discordant zircons are included, spurious Neoproterozoic and Phanerozoic age fractions would be suggested. Even when using the $^{207}Pb/^{206}Pb$ on less than 10% discordant discordant zircon, a spread of ages towards 1000 Ma is indicated, which is not supported by Hf isotope data which suggest that the zircon population in this sample is monogenetic, except for rare, Palaeoproterozoic inheritance.

Table A2 shows pairwise comparisons of the samples in the present study using the likeness and overlap parameters described in the main text applied to the whole data set, incuding discordant grains. These tables should be compared to Tables 2 and 3 in the main text. There are minor changes in L_1, L_2 and O values which are most noticable for pairs including SA12/32 and BS36A, which have the largest fractions of discordant grains, but the the overall pattern of overlap and likeness among the samples remains unchanged.

References for Appendix 2

JELE, N.L. 2014. *The genesis of the quartz-sericite schists of the Toggekry formation, Nondweni greenstone belt, South Africa.* MSc thesis, University of KwaZulu-Natal, 159 pp.

MCCOURT, S., ARMSTRONG, R.A., GRANTHAM, G.H. & THOMAS, R.J. 2006. Geology and evolution of the Natal belt, South Africa. *Journal of African Earth Sciences,* **46**, 71–92.

SPENCER, C.J., THOMAS, R.J., ROBERTS, N-M.W., CAWOOD, P.A., MILLAR, I. @ TAPSTER, S., 2015. Crustal growth during island arc accretion and transcurrent deformation, Natal Metamorphic Province, South Africa: New isotopic constraints. *Precambrian Research*, **265**, 203-217.

ZEH, A. & GERDES, A.H., C. 2013. U−Pb and Hf isotope data of detrital zircons from the Barberton Greenstone Belt: constraints on provenance and Archaean crustal evolution. *Journal of the Geological Society,* **170**, 215-223.

ZEH, A., GERDES, A. & MILLONIG, L. 2013. Hafnium isotopic record of the Ancient Gneiss Complex, Swaziland, southern Africa: evidence for Archaean crust-mantle formation and crust reworking between 3.66 and 2.73 Ga. Journal of the Geological Society, London, **168**, *953-963*.

ZEH, A., GERDES, A., BARTON, J. & KLEMD, R. 2010. U-Th-Pb and Lu-Hf systematics of zircon from TTG's, leucosomes, meta-anorthosites and quartzites of the Limpopo Belt (South Africa): Constraints for the formation, recycling and metamorphism of Palaeoarchaean crust. *Precambrian Research,* **179**, 50-68.

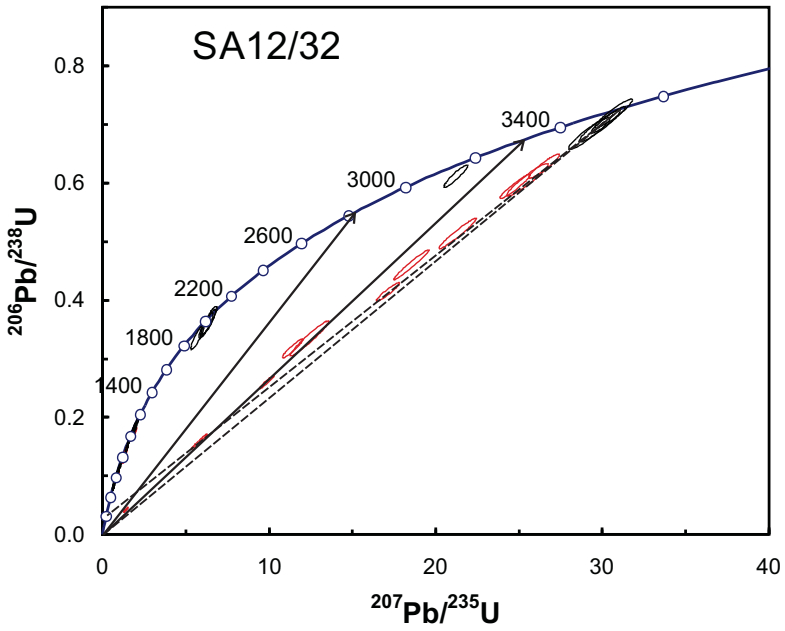
SA12/32
0.8
0.6
0.4
0.2
0.0
0
10
20
30
40
3400
3000
2600
2200
1800
1400
$^{206}Pb/^{238}U$
$^{207}Pb/^{235}U$

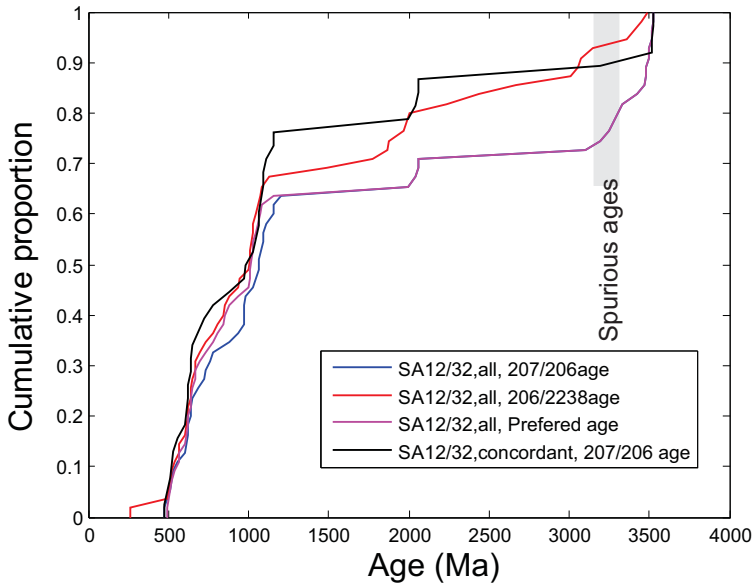
Cumulative proportion
Age (Ma)
Spurious ages
SA12/32,all, 207/206age
SA12/32,all, 206/2238age
SA12/32,all, Prefered age
SA12/32,concordant, 207/206 age

Fig A2a

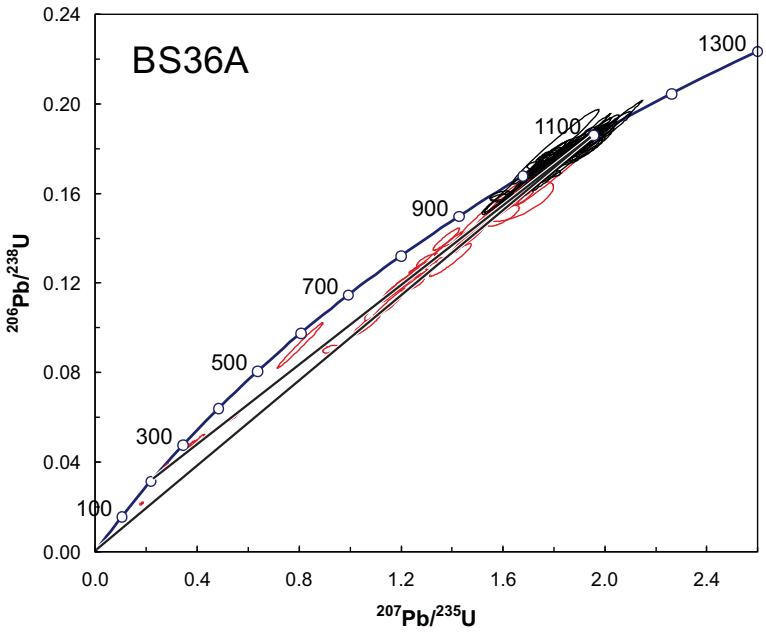
BS36A
1300
1100
900
700
500
300
100
0.24
0.20
0.16
0.12
0.08
0.04
0.00
0.0
0.4
0.8
1.2
1.6
2.0
2.4
$^{206}Pb/^{238}U$
$^{207}Pb/^{235}U$

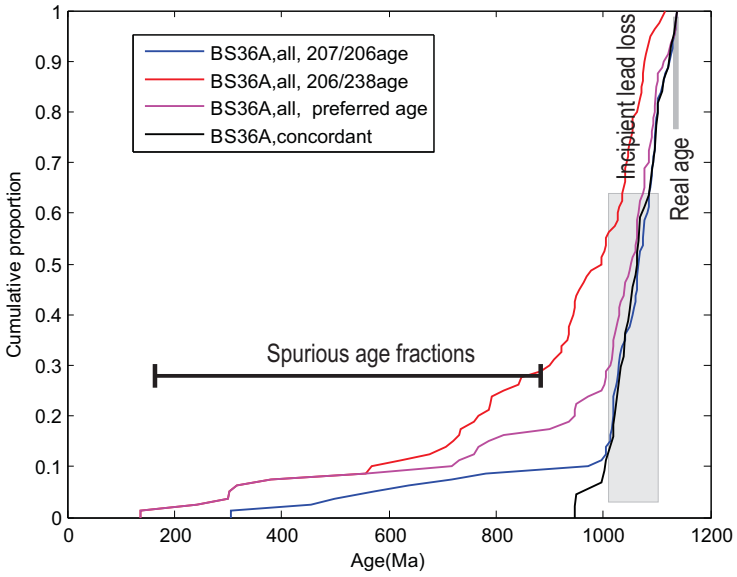
BS36A,all, 207/206age
BS36A,all, 206/238age
BS36A,all, preferred age
BS36A,concordant
Incipient lead loss
Real age
Spurious age fractions
Cumulative proportion
Age(Ma)
0
0.1
0.2
0.3
0.4
0.5
0.6
0.7
0.8
0.9
1
0
200
400
600
800
1000
1200

Fig A2b

Table A1 *Likeness and overlap parameters calculated from the complete datsaset (including discordant zircons).*

L_1	BS36A	C0445	C1690B	DL11A	DL13B	DL13C	SA1201	SA1232	SA1237	RBS	PONG13	Orange	VRY
BES	0.46	0.75	0.75	0.63	0.61	0.62	0.69	0.61	0.73	0.81	0.74	0.64	0.62
BS36A		0.46	0.54	0.29	0.28	0.29	0.72	0.34	0.40	0.53	0.39	0.54	0.29
C0445			0.80	0.72	0.71	0.73	0.68	0.60	0.82	0.83	0.79	0.69	0.72
C1690B				0.65	0.65	0.67	0.75	0.59	0.76	0.87	0.72	0.75	0.67
DL11A					0.76	0.79	0.50	0.51	0.79	0.65	0.72	0.54	0.84
DL13B						0.90	0.48	0.57	0.78	0.65	0.72	0.54	0.87
DL13C							0.50	0.57	0.80	0.67	0.73	0.56	0.89
SA12/01								0.55	0.61	0.74	0.62	0.66	0.49
SA12/32									0.62	0.60	0.68	0.53	0.57
SA12/37										0.78	0.86	0.66	0.81
RBS											0.76	0.73	0.66
PONG13												0.64	0.73

L_2	BS36A	C0445	C1690B	DL11A	DL13B	DL13C	SA1201	SA1232	SA1237	RBS	PONG13	Orange	VRY
BES	0.17	0.60	0.62	0.54	0.47	0.41	0.57	0.46	0.53	0.69	0.55	0.42	0.50
BS36A		0.15	0.19	0.10	0.09	0.08	0.36	0.12	0.10	0.19	0.14	0.35	0.11
C0445			0.71	0.64	0.58	0.55	0.64	0.50	0.61	0.70	0.60	0.49	0.62
C1690B				0.61	0.55	0.52	0.65	0.49	0.63	0.74	0.58	0.54	0.60
DL11A					0.65	0.67	0.47	0.43	0.69	0.58	0.60	0.43	0.73
DL13B						0.71	0.41	0.46	0.69	0.58	0.64	0.43	0.72
DL13C							0.41	0.43	0.71	0.54	0.60	0.44	0.76
SA12/01								0.45	0.51	0.66	0.50	0.54	0.44
SA12/32									0.51	0.49	0.53	0.43	0.50
SA12/37										0.61	0.68	0.46	0.74
RBS											0.58	0.48	0.59
PONG13												0.48	0.64

O	n(all)	BS36A	C0445	C1690B	DL11A	DL13B	DL13C	SA1201	SA1232	SA1237	RBS	PONG13	Orange	VRY
BES	100	0.87	1.00	1.00	1.00	1.00	1.00	1.00	0.75	1.00	1.00	1.00	1.00	1.00
BS36A	80		0.87	0.87	0.86	0.87	0.87	1.00	0.74	0.87	0.88	0.88	1.00	0.85
C0445	80			1.00	1.00	1.00	1.00	1.00	0.91	1.00	1.00	1.00	1.00	1.00
C1690B	108				1.00	1.00	1.00	1.00	0.73	1.00	1.00	1.00	1.00	0.90
DL11A	55					1.00	1.00	0.89	0.89	1.00	1.00	1.00	0.89	1.00
DL13B	80						1.00	0.88	0.61	1.00	1.00	1.00	0.88	1.00
DL13C	65							0.88	0.75	1.00	1.00	1.00	0.88	1.00
SA12/01	74								0.76	0.92	1.00	0.97	1.00	0.87
SA12/32	55									0.71	0.73	0.87	0.97	0.58
SA12/37	103										1.00	1.00	0.95	1.00
RBS	102											1.00	1.00	0.92
PONG13	122												1.00	0.98